

Mechanical enhancement of quantum oscillations

Maximilian Daschner,^{1,2,*} Ivan Kokanović,^{3,1,†} and F. Malte Grosche^{1,‡}

¹*Cavendish Laboratory, University of Cambridge, Cambridge CB3 0HE, United Kingdom*

²*Fakultät für Physik, Ludwig-Maximilians-Universität, München, Germany*

³*Department of Physics, Faculty of Science, University of Zagreb, Zagreb, Croatia*

We investigate quantum oscillation measurements in the Dirac nodal-line semimetal TaNiTe₅ which exhibit a strongly enhanced amplitude in the magnetoresistance. We show that mechanical properties of the measurement setup in combination with de Haas - van Alphen oscillations in the magnetic torque can cause this enhancement in the measured resistance, without involvement of any topological properties in this material. To support the empirical data, a numerical model is provided, showing good agreement.

I. INTRODUCTION

Weyl and Dirac semimetals are materials whose band structure hosts a linear band crossing in the Brillouin zone, usually close to the Fermi energy. These materials have recently gained interest due to their topological properties [1–7]. Novel experimental signatures, some of which include the appearance of Fermi arcs [8] and the presence of the chiral anomaly [9, 10], were first discovered in these materials.

When exposed to strong magnetic fields, metals in general exhibit so-called quantum oscillations that can be probed [11] in various physical properties such as the magnetisation, known as the de Haas - van Alphen (dHvA) effect, or the magnetoresistance (MR), known as the Shubnikov - de Haas (SdH) effect. These oscillations allow to map out the Fermi surface of a material and provide additional information about the effective masses and the nature of electron scattering. What motivates the field of probing quantum oscillations in Dirac semimetals is that under certain circumstances, they obtain a π phase shift which can be directly related to the presence of non-trivial Berry curvature around the Dirac nodal points [12].

Among the various material candidates for Dirac semimetals, the family TaXTe₅ (X = Ni, Pd, Pt) [13–28] falls into the category of Dirac nodal-line semimetals where the linear band crossing is not limited to a single point but extends along a line in the Brillouin zone. In this work we focus on one representative of this family, namely TaNiTe₅, and discuss the strongly amplified quantum oscillations in the magnetoresistance presented in a recent publication by the authors [29]. This strong enhancement suggests the presence of a novel topological signature in Dirac nodal-line semimetals. However, a theoretical model based on classical mechanics and electrodynamics can fully account for this experimental result. A numerical study is also provided and shows good agreement with the empirical data.

II. METHODS

Single crystals of TaNiTe₅ were grown with the self-flux growth method. Elements of Ta, Ni, and Te were mixed together with a molar ratio of Ta:Ni:Te = 1:1:10 inside a glove box filled with purified Argon gas. After filling the mixture into a quartz tube and sealing the tube in vacuum, it was then heated to over 973 K over the course of four days and then cooled to 773 K within a week. Similar to its sister compounds, TaNiTe₅ grows in shiny needle shaped layered single crystals.

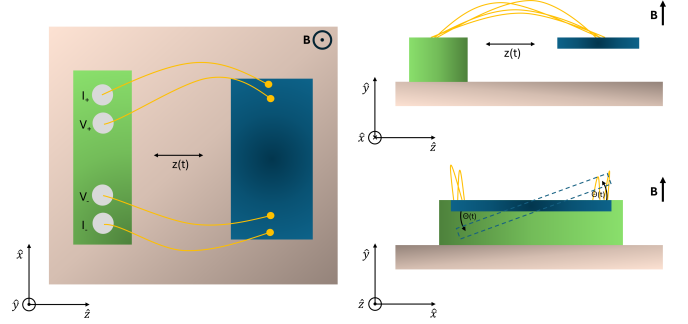


Figure 1. Typical setup of a four-point resistivity measurement of a sample (blue). The gold wires connect the sample with contact pads on a circuit board (green). Voltage (V) and current (I) contact pads from which electronic measurements can be conducted are drawn in grey. An image of a real setup as used in the 9 T-PPMS is shown in Appendix A. The crystallographic axes a , b and c of TaNiTe₅ are aligned with \hat{x} , \hat{y} and \hat{z} , respectively.

Measurements shown here were performed in a Quantum Design Physical Property Measurement System (PPMS) with a 14 T magnet (referred to as the 14 T-PPMS), and a PPMS with a 9 T magnet (referred to as the 9 T-PPMS). A typical four-point measurement inside the cryostat is sketched in Figure 1. The sample is held up by gold wires and thus floating, such that it can freely move if exposed to a force. The only relevant degrees of freedom here are given by the lateral movement in $\mathbf{z}(\mathbf{t})$ and a rotational movement in the \hat{x} - \hat{y} plane by an angle $\theta(t)$. All transport measurement were performed with a SR830 lock-in amplifier.

* md867@cam.ac.uk; maximilian.daschner@lmu.de

† kivan@phy.hr

‡ fmg12@cam.ac.uk

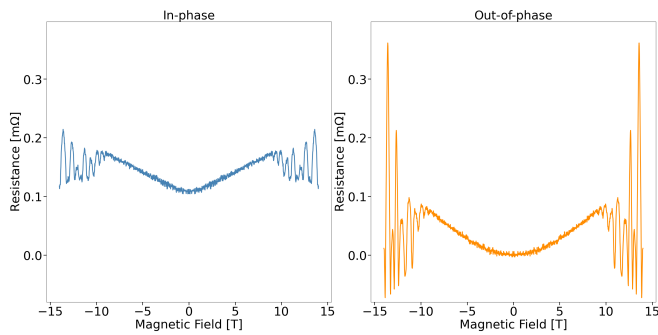


Figure 2. Magnetoconductance measurement of a TaNiTe₅ sample where $I \parallel \hat{x}$ and $B \parallel \hat{y}$ (in Figure 1). Data is split into the in-phase (left) and out-of-phase (right) components. This data was measured in a 14 T-PPMS at 1.8 K.

III. EXPERIMENTAL RESULTS

Figure 2 shows a measurement of SdH oscillations in a TaNiTe₅ sample, which was performed in a 14 T-PPMS with I parallel to the crystallographic a axis (\hat{x} in Figure 1) and B parallel to the crystallographic b axis (\hat{y} in Figure 1). Voltage contacts were not aligned in a straight line and hence a Hall component showed up in the measurement data. The longitudinal resistance $R(B)$ data was corrected for the Hall component by symmetrising via

$$R = \frac{R(B) + R(-B)}{2} \quad (1)$$

Generally, a lock-in amplifier applies a periodic current with a frequency and phase shift that it can use to amplify the measured voltage drop across the sample. The measured signal can be separated into an oscillation that is in phase with the reference signal, and one that is shifted by $\pi/2$ with respect to the reference signal of the lock-in amplifier, and is thus out of phase. We should expect the vast majority of the input signal to be in phase with the reference signal unless inductive or capacitive effects are present. Figure 2 shows an enhanced signal in these components both of which host strongly amplified quantum oscillations, with the out-of-phase component even obtaining negative values at high magnetic fields. At fields between -9 T to 9 T the resistance in the in-phase component shows semiclassical behaviour, while the out-of-phase component increases quadratically in field. Both components show a drop at fields beyond ± 9 T with continuously increasing quantum oscillations. To investigate the origin of this peculiar effect, the measurements were repeated in the 9 T-PPMS with the same sample, again with $I \parallel a$ and $B \parallel b$, and the temperature-dependent magnetoconductance defined in terms of longitudinal resistance $R(B)$

$$\text{MR} = \frac{R(B) - R(0)}{R(0)} \quad (2)$$

is illustrated in Figure 3. Higher resolution was ob-

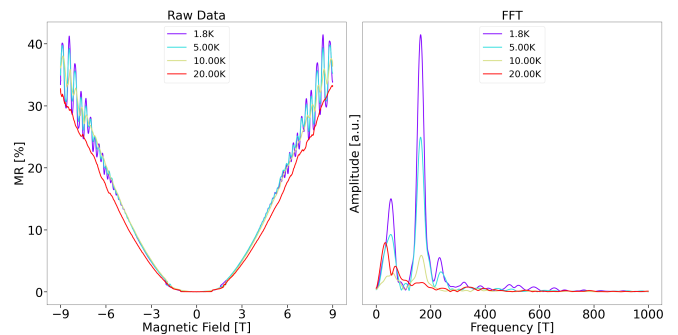


Figure 3. Left: Magnetoconductance of a TaNiTe₅ sample at various temperatures. Total magnetoconductance derived from the in-phase (IP) and out-of-phase (OOP) resistances via $R = \sqrt{R_{\text{IP}}^2 + R_{\text{OOP}}^2}$ is shown here. The frequency on the lock-in amplifier was set to 11 Hz. Right: Respective fast Fourier transforms.

tained in this measurement which allowed for the analysis of quantum oscillations. We find frequencies of 53.0(3) T, 163.0(4) T and 233(3) T with effective masses of 0.14(2) m_e , 0.23(1) m_e and 0.23(3) m_e , respectively. The Dingle temperature for the first two frequencies could be determined as 12.9(4) K and 14.7(3) K respectively, while the data for the third frequency did not allow for determination of the Dingle temperature. Overall agreement with the literature [13, 18, 21, 29] is good and this data provides evidence of Shubnikov - de Haas oscillations, which so far have only been reported at much higher fields of up to 30 T [21] or even up to 50 T [13].

Given that the frequencies and effective masses are consistent with DFT calculations and results from previous measurements [29], these strongly amplified oscillations seem to fundamentally originate from the Fermi surface of this material. The purity of the crystals used here can be ruled out as a potential cause for this enhancement as the residual resistance ratio (RRR) is close to the value in the literature ($\text{RRR} \approx 25$). Even with a high RRR, the purity of the crystals alone is not enough to explain the large out-of-phase component. Spot-welded gold wires and gold wires attached to the sample with silver epoxy have both shown amplified oscillations, indicating that this effect is not a result of the wiring. In particular any chemical reaction between the silver epoxy and the sample surface does not contribute to these oscillations.

To perform a more thorough analysis of the data shown in Figure 3, the low-temperature data was split into its in-phase and out-of-phase components similar to the data obtained in the 14 T-PPMS as illustrated in Figure 4. Note that for the out-of-phase component the resistance at $B = 0$ is zero, and since the magnetoconductance is only well-defined if $R(0) \neq 0$, the resistance $R(B)$ is given instead of MR in this case. Apart from its quadratic dependence on the magnetic field, the magnetoconductance of the in-phase component also shows a quadratic dependence on the frequency of the reference signal set on

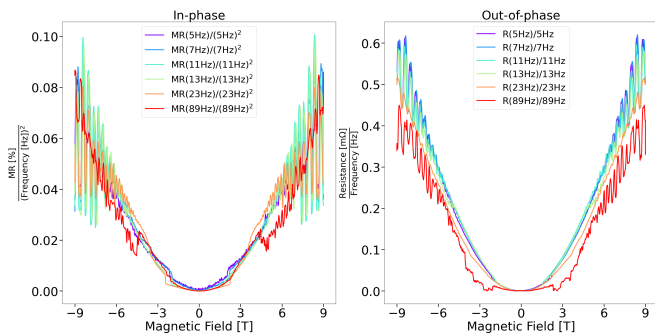


Figure 4. Data from Figure 3 measured at 1.8 K split into the in-phase and out-of-phase component of the lock-in amplifier. Since the out-of phase component is zero at 0 T, the resistance is shown instead of the MR in this case.

the lock-in amplifier, which is evident when dividing the data by the square of that frequency. The resistance of the out-of-phase component is also quadratic in B , but shows a linear dependence on the frequency of the reference signal. At higher frequencies (~ 89 Hz) this dependence seems to diverge from the linear relationship, indicating that the linearity only holds to first order.

Motivated by the occurrence of mechanical signatures such as resonance peaks in measurements of TaNiTe_5 and other materials even at room temperature (see Appendix B), the quantum oscillation data shown here can possibly be explained by the interplay of classical and quantum effects. To verify this hypothesis, samples of TaNiTe_5 were measured such that mechanical movement would either be allowed or restricted. A series of measurements started with a free floating sample which is only held by the gold wires attached to it with the current and magnetic field again as sketched in Figure 1. After the first field sweep, the sample is taken out of the 9 T-PPMS and firmly attached to the bottom of the measurement puck with vacuum grease before being cooled down and measured in another field sweep. The sample is then again taken out of the cryostat, detached from the vacuum grease so that it is only held up by the gold wires, and the process repeats. Field sweeps with samples that are floating freely show strong quantum oscillations as illustrated in Figure 5, while field sweeps with samples that are attached to the puck with vacuum grease do not show any oscillations at all. Furthermore, a strong out-of-phase component arises only in field sweeps with detached samples and obtains values much larger than the in-phase component which leads to the conclusion that this strong out-of-phase component and the presence of quantum oscillations are related in some way.

IV. THEORETICAL MODEL

To explain this strange behaviour, a simple model based on damped harmonic oscillators as motivated in Appendix B can be used. Figure 1 shows a regular setup

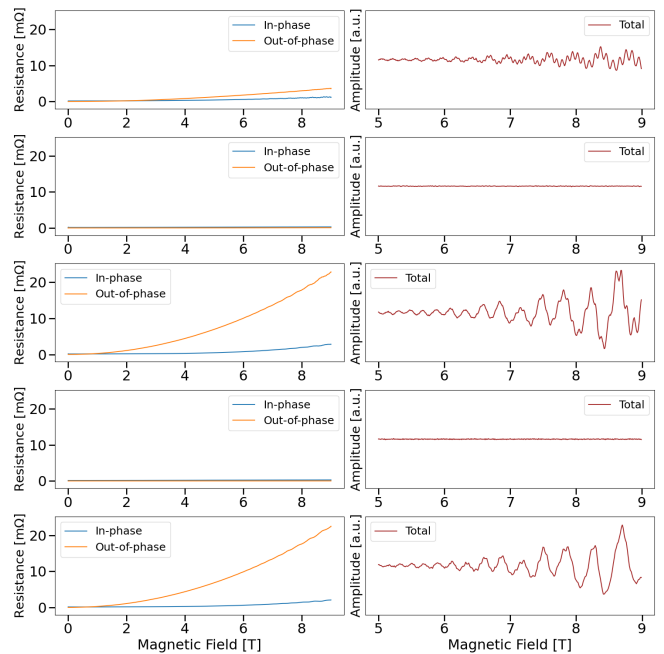


Figure 5. Relation between enhancement of quantum oscillations and mechanical movement. Left: Resistance in field of a TaNiTe_5 sample that is either solely held up by thin gold wires (first, third and fifth row) or attached to the measurement puck using vacuum grease (second and fourth row) measured at 1.8 K. Directions of current and magnetic field are $I \parallel a$ and $B \parallel b$. Right: Background subtracted data, where the total data shown here includes the in-phase and out-of-phase components. The scale is identical in all figures, i.e. despite being arbitrary, the units are the same in all figures.

of a four-point measurement with the gold wires simultaneously measuring and holding up a sample of length L , where we can neglect gravity due to the relatively low weight of the sample compared to the spring constant of the wires. We thus have a floating sample through which an AC current $I(t)$ proportional to the voltage

$$V(t) = V_0 \sin(\omega t) \quad (3)$$

is flowing inside an external magnetic field. Here V_0 is the amplitude and ω is the frequency of the signal applied by the lock-in amplifier. The sample can be approximated by a straight, sturdy, one-dimensional rod whose length is parametrised by

$$\mathbf{L} = L \hat{\mathbf{L}} = L \begin{pmatrix} \cos(\theta_0 + \theta(t)) \\ \sin(\theta_0 + \theta(t)) \\ 0 \end{pmatrix} \quad (4)$$

while the magnetic field is given by $\mathbf{B} = B\hat{\mathbf{y}}$.

Since a current is flowing through the sample inside a magnetic field, it is affected by the Lorentz force

$$\begin{aligned} \mathbf{F}_{\mathbf{L}} &= I(t)\mathbf{L} \times \mathbf{B} = I(t)BL \hat{\mathbf{L}} \times \hat{\mathbf{y}} \\ &= I(t)BL \cos(\theta_0 + \theta(t)) \hat{\mathbf{z}} \end{aligned} \quad (5)$$

that pushes the sample either in the $+\hat{z}$ or $-\hat{z}$ direction depending on the direction of the current. The current is along \hat{x} unless the sample rotates in space to an angle $\theta_0 + \theta(t)$ which would reduce the Lorentz force due to the cosine term. We assume that the sample is initially tilted by a small angle θ_0 , and can rotate further by an angle of $\theta(t)$. Sources that induce such rotation will be discussed later.

As a result of the Lorentz force, the sample is expected to oscillate back and forth at the frequency of the AC current, where the spring constant of the gold wires act as a damping term in the equation of motion (e.o.m.) which we will set up shortly. Now, whenever a metallic sample is moving in a magnetic field, independent of the exact cause of such movement, we should also expect an induced voltage

$$\begin{aligned} U_I(t) &= (\dot{\mathbf{r}}(t) \times \mathbf{B}) \cdot \mathbf{L} = -\dot{z}(t)BL \hat{x} \cdot \hat{\mathbf{L}} \\ &= -\dot{z}(t)BL \cos(\theta_0 + \theta(t)) \end{aligned} \quad (6)$$

inside the sample, which is proportional to the velocity along \hat{z} . This induced voltage will be measured by the voltage contacts together with the magnetoresistance of the sample as sketched in Figure 6. Equation 5 and Equation 6 indicate that the amplitude of both, the induced voltage and the Lorentz force, is strongly dependent on the angle between the current I and the magnetic field B . If a torque was present that tilts the orientation of the sample by $\theta(t)$, while the sample is constantly oscillating back and forth due to the AC current, both the Lorentz force and the induced voltage would be lowered. A potential candidate for such a torque is given by de Haas - van Alphen oscillations in the magnetic torque that can indeed cause a sample to tilt in field. Such torque τ_{QO} is just given [30] as

$$\tau_{QO}(\theta, B) \propto B^{\frac{3}{2}} R_T R_D R_S \sin\left(2\pi\left(\frac{F(\theta)}{B} - \gamma\right) \pm \delta\right) \quad (7)$$

if only one orbit and one harmonic are taken into account. Here, R_x ($x=T,D,S$) are various damping terms, while $F(\theta)$ is the frequency arising from the respective Fermi surface and B the magnetic field. γ and δ are shifts associated with the Berry phase and the dimensionality of the system and play very little role in the model considered here and will thus be neglected. Note that in case the sample made a 180° turn, Equation 5 and Equation 6 remain correct, however the contacts of the gold wires flip as well, and hence the resulting sign change needs to be incorporated in this model. This can be done by taking the absolute value of the cosine in Equation 6.

The underlying principle of this model is that the measurements of quantum oscillations in the resistivity, also known as Shubnikov - de Haas oscillations, shown here are in reality measurements of the induced voltage through the constant back and forth movement of the sample along \hat{z} and its reduction or increase due to the rotation of the sample in the \hat{x} - \hat{y} plane caused by de Haas - van Alphen oscillations in the magnetic torque. Given this qualitative understanding, we can attempt to

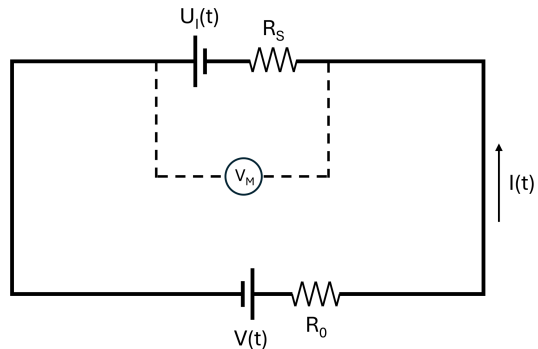


Figure 6. Simple circuit diagram for a four-point measurement of a sample with resistance R_S including an additional induced voltage $U_I(t)$. A lock-in amplifier generates a sinusoidal voltage $V(t)$ and measures a voltage V_M . The total resistance of the circuit includes a resistor $R_0 = 1 \text{ k}\Omega$ in series that was put in place to reduce the current, the resistance of the wires, and the resistance of the sample.

continue with the model by motivating two equations of motion for the movement and tilt of the sample. We introduced $z(t)$ as the only degree of freedom that describes the movement of the centre of mass, since movements in the \hat{x} and \hat{y} direction do not contribute to the induced voltage. Furthermore, we introduced the angle $\theta(t)$ which describes the orientation of the sample in the \hat{x} - \hat{y} plane. In what follows, we will motivate equations of motion for each of these two degrees of freedom, both of which will be based on damped harmonic oscillators. They will then be coupled which allows us to derive an expression for the overall induced voltage in the sample. We begin with the angle $\theta(t)$, since it can be solved independently of the lateral movement along \hat{z} . Once an expression for $\theta(t)$ is derived, it can be used to find $z(t)$ which can then be used to find an explicit expression for $U_I(t)$ in Equation 6. Together with the sample's inherent magnetoresistance R_S , we propose that this is what is measured in the empirical data shown here.

The angle $\theta(t)$ is only affected by the magnetic torque arising from quantum oscillations, which are damped due to the presence of gold wires attached to the sample (see Figure 1) acting as springs. It represents the orientation of the sample and can be described by a damped harmonic oscillator:

$$J\ddot{\theta}(t) = \tau_{QO}(\theta(t), t) - k_1\theta(t) - k_2\dot{\theta}(t) \quad (8)$$

where t is the time, J is the moment of inertia, k_1 and k_2 are damping constants. Given that the magnetic field is ramped up comparatively slowly ($B_{\text{rate}} \approx 0.1 \text{ T min}^{-1}$), we can neglect the first and second derivatives such that Equation 8 becomes

$$\theta(t) \approx \theta = \frac{\tau_{QO}(\theta, B)}{k_1} \quad (9)$$

where the magnetic field B can be related to time through $B = B_{\text{rate}} \cdot t$. At any given field, we thus assume that the

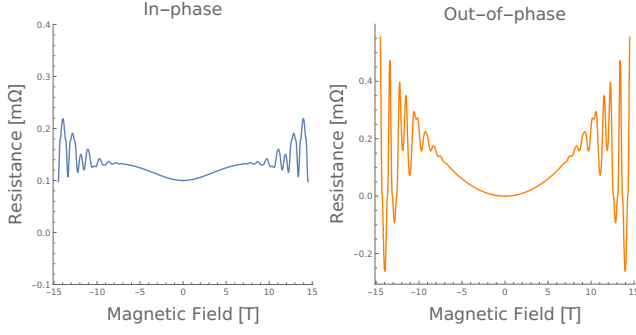


Figure 7. Numerical evaluation of Equation 15 and Equation 16 closely resembling Figure 2.

orientation of the sample will instantaneously align at an angle which can be found using the equation above. Note that since $\tau_{QO}(\theta, B)$ also depends on the angle, which it does in general since the frequency is angle-dependent, solving the above equation can become complicated. Nonetheless, the problem of solving a differential equation was reduced to solving an algebraic equation which is in general much simpler. For reasons of numerical stability, we will assume that the frequency F is angle-independent from here on.

The equation of motion for the centre of mass movement along $\hat{\mathbf{z}}$ can be described by a driven, damped harmonic oscillator involving the Lorentz force \mathbf{F}_L and damping terms κ_1 and κ_2 arising from the gold wires:

$$m\ddot{\mathbf{r}}(t) = \mathbf{F}_L - \kappa_1\dot{\mathbf{r}}(t) - \kappa_2\dot{\mathbf{r}}(t) \quad (10)$$

$$m\ddot{z}(t) \hat{\mathbf{z}} = [I(t)BL \cos(\theta_0 + \theta) - \kappa_1 z(t) - \kappa_2 \dot{z}(t)] \hat{\mathbf{z}} \quad (11)$$

where the centre of mass of the sample is only moving along the $\hat{\mathbf{z}}$ direction. The periodic Lorentz force is driven by the periodic current from the lock-in amplifier. In principle, the current $I(t)$ itself also needs to be modified since the movement of the sample will induce a voltage that does not only affect the measurement, but also the current flowing through the circuit. This would lead to a set of coupled equations of motion, since the modified current $I(t)$ in turn also impacts the movement of the sample through Equation 11. However, we can safely assume that the current $I(t)$ is dominated by the lock-in amplifier, i.e. $V(t) \gg U_I(t)$, hence the current can be expressed by

$$I(t) = \frac{1}{R_0}(V(t) + U_I(t)) \approx \frac{1}{R_0}V(t) = \frac{V_0}{R_0} \sin(\omega t) \quad (12)$$

Since the resistance of the wires and of the sample are orders of magnitude smaller than R_0 (see Figure 6), they will both be neglected here. The goal is to solve the e.o.m. for $z(t)$ in Equation 11 to obtain $U_I(t)$ in Equation 6. The measured voltage V_M is then given by

$$V_M(t) = I(t)R_S(B) + U_I(t) \quad (13)$$

which is just a modification of the sample resistance with the induced voltage. The sample resistance $R_S(B)$ in

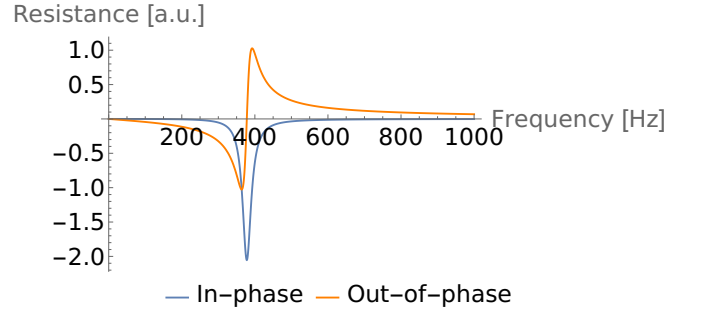


Figure 8. Mechanical resonance measured in the resistance described by Equation 15 and Equation 16. The resonant frequency can be determined using Equation 19.

field is assumed to show semiclassical behaviour which can simply be expressed [31–36] as

$$R_S(B) = R_S(0) + R_S(0) \frac{\alpha B^2}{\beta + B^2} \quad (14)$$

where α and β are material-dependent parameters that can be determined from a stationary sample. Note that it will be the induced voltage $U_I(t)$ that introduces the pronounced quantum oscillations both in the in-phase and out-of-phase component measured by the lock-in amplifier. After solving the second order differential equation in Equation 11 and using it in $V_M(t)$, the result can then be grouped by terms proportional to $\sin(\omega t)$ and $\cos(\omega t)$ to obtain the in-phase (IP) and out-of-phase (OOP) components, which leads to

$$V_M^{\text{IP}} = \frac{V_0}{R_0} \left(R_S - \frac{\kappa_2 \omega^2 B^2 l^2 \cos(\theta_0 + \theta) |\cos(\theta_0 + \theta)|}{\kappa_1^2 + m^2 \omega^4 - 2\kappa_1 m \omega^2 + \kappa_2^2 \omega^2} \right) \quad (15)$$

$$V_M^{\text{OOP}} = \frac{V_0}{R_0} \frac{(m\omega^2 - \kappa_1) \omega B^2 l^2 \cos(\theta_0 + \theta) |\cos(\theta_0 + \theta)|}{\kappa_1^2 + m^2 \omega^4 - 2\kappa_1 m \omega^2 + \kappa_2^2 \omega^2} \quad (16)$$

with the corresponding results being illustrated in Figure 7, showing strong resemblance with the data in Figure 2. To compare this model to the measurement data further, we can generate a power series expansion of Equation 15 and Equation 16 to lowest order in the frequency ω :

$$V_M^{\text{IP}} \approx R_S \frac{V_0}{R_0} - \frac{V_0}{R_0} \frac{\kappa_2 l^2}{\kappa_1^2} \cos\left(\theta_0 + \frac{\tau_{QO}}{k_1}\right) \left| \cos\left(\theta_0 + \frac{\tau_{QO}}{k_1}\right) \right| B^2 \omega^2 \quad (17)$$

$$V_M^{\text{OOP}} \approx -\frac{V_0}{R_0} \frac{l^2}{\kappa_1} \cos\left(\theta_0 + \frac{\tau_{QO}}{k_1}\right) \left| \cos\left(\theta_0 + \frac{\tau_{QO}}{k_1}\right) \right| B^2 \omega \quad (18)$$

which confirms the quadratic and linear frequency dependences measured in the in-phase and out-of-phase components in Figure 4, respectively. The slight deviation from these power laws at higher frequencies in the measurement data could either be due to higher order terms or due to non-linear effects in the gold wires. Furthermore, we can see that the dependence on the magnetic field is quadratic, which was also observed in the raw data.

The resonance frequency ω_R can be found by determining the zeros of either Equation 16 or the derivative of Equation 15, each of which leads to

$$\omega_R = \sqrt{\frac{\kappa_1}{m}} \quad (19)$$

This resonance can be reproduced in the in-phase and out-of-phase components as illustrated in Figure 8 at a fixed magnetic field. It strongly resembles the resonance peaks observed in Figure 10 b) up to a sign.

V. CONCLUSION

We discuss the occurrence of a novel mechanical effect that amplifies the magnitude of quantum oscillations. A simple model based on a driven, damped harmonic oscillator, with the applied current acting as the driving force and the gold wires introducing damping, is able to explain the results accurately, and no topological properties need to be invoked. The model presented here is consistent with a number of properties measured in samples of TaNiTe₅. Both the in-phase and out-of-phase magnetoresistances show quadratic behaviour in field, and depend quadratically and linearly on the frequency of the reference signal from the lock-in amplifier, respectively.

Future experimental studies of Dirac semimetals, and possibly metals more generally, should take these results into account when performing Shubnikov - de Haas measurements.

ACKNOWLEDGMENTS

M. Daschner would like to thank Jiasheng Chen for many discussions regarding the nature of these strong quantum oscillations.

Appendix A: Image of a real setup in the 9 T-PPMS



Figure 9. Two TaNiTe₅ samples on a standard Quantum Design measurement puck. Note how both of them are held by the gold wires alone, thus floating above the platform.

Appendix B: Mechanical resonance in magnetic field

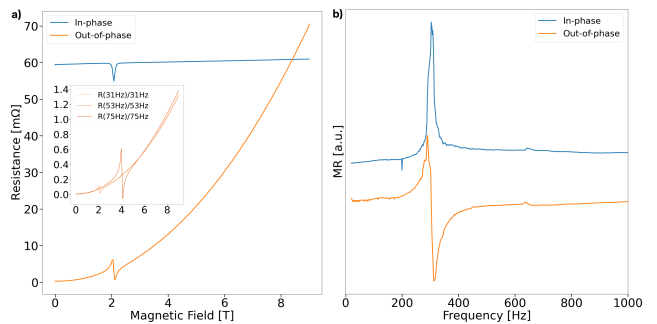


Figure 10. a) Field sweep of a Fe₃GeTe₂ sample at 53 Hz and 300.0 K. The inset shows the out-of-phase component for different frequencies divided by the respective frequency. b) Frequency sweep of a TaNiTe₅ at 13 T and 1.5 K. Both components resemble the behaviour of a damped harmonic oscillator known from classical mechanics.

The strong out-of-phase component with its linear frequency-dependence in the main text was also observed in other materials whenever the respective samples had not been firmly attached to the measurement platform. This effect was present even at room temperature measured in the 9 T-PPMS as is illustrated with a sample of Fe₃GeTe₂ shown in Figure 10 a). While the in-phase component increases only slightly in magnetic field, which is expected for such a measurement at room temperature, the out-of-phase component increases $\propto B^\alpha$ with $\alpha = 2.091(2)$ and thus nearly quadratically in field. Furthermore, the inset clearly shows a linear dependence on the frequency of the reference signal. Interestingly, this data also shows the presence of a resonance peak emerging at around 2 T both in the in-phase and out-of-phase components, strongly resembling the physics of a damped harmonic oscillator. The position of this resonance peak seems to shift as the frequency is altered which is illustrated in the inset in Figure 10 a). To see if these resonance peaks also appear in TaNiTe₅, a sample of this material was measured in a custom-designed Oxford Instruments cryostat at 1.5 K in a constant external magnetic field of 13 T, and the frequency was slowly increased (8 Hz min⁻¹), with the results given in Figure 10 b). Upon increasing the frequency on the lock-in amplifier a clear resonance peak becomes visible, reminiscent of what was observed in Fe₃GeTe₂ when the magnetic field was swept at constant frequency. These results further confirm the presence of mechanical effects in these measurements.

- [1] BQ Lv, T Qian, and H Ding. Experimental perspective on three-dimensional topological semimetals. *Reviews of Modern Physics*, 93(2):025002, 2021.
- [2] NP Armitage, EJ Mele, and Ashvin Vishwanath. Weyl and Dirac semimetals in three-dimensional solids. *Reviews of Modern Physics*, 90(1):015001, 2018.
- [3] Binghai Yan and Claudia Felser. Topological materials: Weyl semimetals. *Annual Review of Condensed Matter Physics*, 8:337–354, 2017.
- [4] Di Xiao, Ming-Che Chang, and Qian Niu. Berry phase effects on electronic properties. *Reviews of modern physics*, 82(3):1959, 2010.
- [5] NP Ong and Sihang Liang. Experimental signatures of the chiral anomaly in Dirac-Weyl semimetals. *Nature Reviews Physics*, 3(6):394–404, 2021.
- [6] Shuo Wang, Ben-Chuan Lin, An-Qi Wang, Da-Peng Yu, and Zhi-Min Liao. Quantum transport in Dirac and Weyl semimetals: a review. *Advances in Physics: X*, 2(3):518–544, 2017.
- [7] M Zahid Hasan and Charles L Kane. Colloquium: topological insulators. *Reviews of modern physics*, 82(4):3045, 2010.
- [8] Su-Yang Xu, Ilya Belopolski, Nasser Alidoust, Madhab Neupane, Guang Bian, Chenglong Zhang, Raman Sankar, Guoqing Chang, Zhujun Yuan, Chi-Cheng Lee, et al. Discovery of a Weyl fermion semimetal and topological Fermi arcs. *Science*, 349(6248):613–617, 2015.
- [9] Xiaochun Huang, Lingxiao Zhao, Yujia Long, Peipei Wang, Dong Chen, Zhanhai Yang, Hui Liang, Mianqi Xue, Hongming Weng, Zhong Fang, et al. Observation of the chiral-anomaly-induced negative magnetoresistance in 3D Weyl semimetal TaAs. *Physical Review X*, 5(3):031023, 2015.
- [10] Jun Xiong, Satya K Kushwaha, Tian Liang, Jason W Krizan, Max Hirschberger, Wudi Wang, Robert Joseph Cava, and Nai Phuan Ong. Evidence for the chiral anomaly in the Dirac semimetal Na_3Bi . *Science*, 350(6259):413–416, 2015.
- [11] David Shoenberg. *Magnetic oscillations in metals*. Cambridge university press, 2009.
- [12] GP Mikitik and Yu V Sharlai. Manifestation of Berry’s phase in metal physics. *Physical review letters*, 82(10):2147, 1999.
- [13] Chunqiang Xu, Yi Liu, Pinggen Cai, Bin Li, Wenhe Jiao, Yunlong Li, Junyi Zhang, Wei Zhou, Bin Qian, Xuefan Jiang, et al. Anisotropic transport and quantum oscillations in the quasi-one-dimensional TaNiTe_5 : evidence for the nontrivial band topology. *The Journal of Physical Chemistry Letters*, 11(18):7782–7789, 2020.
- [14] De-Yang Wang, Qi Jiang, Kenta Kuroda, Kaishu Kawaguchi, Ayumi Harasawa, Koichiro Yaji, Arthur Ernst, Hao-Ji Qian, Wen-Jing Liu, He-Ming Zha, et al. Coexistence of strong and weak topological orders in a quasi-one-dimensional material. *Physical Review Letters*, 129(14):146401, 2022.
- [15] Eric W Liimatta and James A Ibers. Synthesis, structures, and conductivities of the new layered compounds $\text{Ta}_3\text{Pd}_3\text{Te}_{14}$ and TaNiTe_5 . *Journal of Solid State Chemistry*, 78(1):7–16, 1989.
- [16] Jiyu Hu, Zhenxiang Dai, Xucai Kan, Ganhong Zheng, Zheng Chen, and Yongqing Ma. Transport and thermal properties of single crystal TaNiTe_5 . *Journal of Alloys and Compounds*, 895:162563, 2022.
- [17] Ni Ma, De-Yang Wang, Ben-Rui Huang, Kai-Yi Li, Jing-Peng Song, Jian-Zhong Liu, Hong-Ping Mei, Mao Ye, and Ang Li. Quasi-one-dimensional characters in topological semimetal TaNiTe_5 . *Chinese Physics B*, 32(5):056801, 2023.
- [18] Rongli Ye, Tian Gao, Haoyu Li, Xiao Liang, and Guixin Cao. Anisotropic giant magnetoresistance and de Haas-van Alphen oscillations in layered topological semimetal crystals. *AIP Advances*, 12(4), 2022.
- [19] Yalei Huang, Rongli Ye, Weihao Shen, Xinyu Yao, and Guixin Cao. Magnetic field-induced resistivity upturn and non-topological origin in the quasi-one-dimensional semimetals. *Symmetry*, 15(10):1882, 2023.
- [20] Yunlong Li, Zhao Ran, Chaozhi Huang, Guanyong Wang, Peiyue Shen, Haili Huang, Chunqiang Xu, Yi Liu, Wenhe Jiao, Wenxiang Jiang, et al. Coexistence of ferroelectric like polarization and Dirac-like surface state in TaNiTe_5 . *Physical Review Letters*, 128(10):106802, 2022.
- [21] Zheng Chen, Min Wu, Yong Zhang, Jinglei Zhang, Yong Nie, Yongliang Qin, Yuyan Han, Chuanying Xi, Shuaiqi Ma, Xucai Kan, et al. Three-dimensional topological semimetal phase in layered TaNiTe_5 probed by quantum oscillations. *Physical Review B*, 103(3):035105, 2021.
- [22] Zhanyang Hao, Weizhao Chen, Yuan Wang, Jiayu Li, Xiao-Ming Ma, Yu-Jie Hao, Ruie Lu, Zecheng Shen, Zhicheng Jiang, Wanling Liu, et al. Multiple Dirac nodal lines in an in-plane anisotropic semimetal TaNiTe_5 . *Physical Review B*, 104(11):115158, 2021.
- [23] Ding-Bang Zhou, Kuang-Hong Gao, Meng-Fan Zhao, Zhi-Yan Jia, Xiao-Xia Hu, Qian-Jin Guo, Hai-Yan Du, Xiao-Ping Chen, and Zhi-Qing Li. Origin of giant magnetoresistance in layered nodal-line semimetal TaNiTe_5 nanoflakes. *arXiv preprint arXiv:2402.16088*, 2024.
- [24] Qi Lu, Zhao Ran, Yunlong Li, Chenhang Xu, Jiayuan Hu, Xunqing Yin, Guohua Wang, Wentao Zhang, Weidong Luo, Xiaofeng Xu, et al. Topologically protected surface states in TaPdTe_5 . *Quantum Frontiers*, 1(1):9, 2022.
- [25] Wen-He Jiao, Xiao-Meng Xie, Yi Liu, Xiaofeng Xu, Bin Li, Chun-Qiang Xu, Ji-Yong Liu, Wei Zhou, Yu-Ke Li, Hai-Yang Yang, et al. Topological Dirac states in a layered telluride TaPdTe_5 with quasi-one-dimensional PdTe_2 chains. *Physical Review B*, 102(7):075141, 2020.
- [26] Arthur Mar and James A Ibers. Synthesis, structure, and physical properties of the new layered ternary telluride TaPtTe_5 . *Journal of Solid State Chemistry*, 92(2):352–361, 1991.
- [27] Shaozhu Xiao, Wen-He Jiao, Yu Lin, Qi Jiang, Xiufu Yang, Yunpeng He, Zhicheng Jiang, Yichen Yang, Zhengtai Liu, Mao Ye, et al. Dirac nodal lines in the quasi-one-dimensional ternary telluride TaPtTe_5 . *Physical Review B*, 105(19):195145, 2022.
- [28] Wen-He Jiao, Shaozhu Xiao, Bin Li, Chunqiang Xu, Xiao-Meng Xie, Hang-Qiang Qiu, Xiaofeng Xu, Yi Liu, Shi-Jie Song, Wei Zhou, et al. Anisotropic transport and de Haas-van Alphen oscillations in quasi-one-dimensional TaPtTe_5 . *Physical Review B*, 103(12):125150, 2021.
- [29] Maximilian Daschner, Friedrich Malte Grosche, Cheng Liu, Bruno Gudac, Mario Novak, and Ivan Kokanović. Probing the Fermi surface with quantum oscillation

- measurements in the Dirac semimetal TaNiTe₅. *arXiv preprint arXiv:2403.12921*, 2024.
- [30] David Shoenberg. The Fermi surfaces of copper, silver and gold. i. the de Haas-van Alphen effect. *Philosophical Transactions of the Royal Society of London. Series A, Mathematical and Physical Sciences*, 255(1052):85–133, 1962.
- [31] Alfred Brian Pippard. *Magnetoresistance in metals*, volume 2. Cambridge university press, 1989.
- [32] Mazhar N Ali, Jun Xiong, Steven Flynn, Jing Tao, Quinn D Gibson, Leslie M Schoop, Tian Liang, Neel Haldolaarachchige, Max Hirschberger, Nai Phuan Ong, et al. Large, non-saturating magnetoresistance in WTe₂. *Nature*, 514(7521):205–208, 2014.
- [33] Fazel Fallah Tafti, Quinn Gibson, Satya Kushwaha, Jason W Krizan, Neel Haldolaarachchige, and Robert Joseph Cava. Temperature- field phase diagram of extreme magnetoresistance. *Proceedings of the National Academy of Sciences*, 113(25):E3475–E3481, 2016.
- [34] YL Wang, LR Thoutam, ZL Xiao, J Hu, S Das, ZQ Mao, J Wei, R Divan, A Luican-Mayer, GW Crabtree, et al. Origin of the turn-on temperature behavior in WTe₂. *Physical Review B*, 92(18):180402, 2015.
- [35] I Pallecchi, Fabio Bernardini, M Tropeano, A Palenzona, A Martinelli, C Ferdeghini, M Vignolo, S Masidda, and M Putti. Magnetotransport in La(Fe, Ru)AsO as a probe of band structure and mobility. *Physical Review B—Condensed Matter and Materials Physics*, 84(13):134524, 2011.
- [36] Kefeng Wang and C Petrovic. Multiband effects and possible Dirac states in LaAgSb₂. *Physical Review B—Condensed Matter and Materials Physics*, 86(15):155213, 2012.